Article:

Sabet, S.A. and de Borst, R. orcid.org/0000-0002-3457-3574 (2019) Mesh bias and shear band inclination in standard and non-standard continua. Archive of Applied Mechanics, 89 (12). pp. 2577-2590. ISSN 0939-1533

https://doi.org/10.1007/s00419-019-01593-2

Noname manuscript No.
(will be inserted by the editor)

Mesh bias and shear band inclination in standard and non-standard continua

Sepideh Alizadeh Sabet · René de Borst

Received: date / Accepted: date

Abstract A severe, spurious dependence of numerical simulations on the mesh size and orientation can be observed in elasto-plastic models with a non-associated flow rule. This is due to the loss of ellipticity, and may also cause a divergence in the incremental-iterative solution procedure. This paper first analyses the dependence of the shear-band inclination in a biaxial test on the mesh size as well as on the mesh orientation. Next, a Cosserat continuum model, which has been employed successfully for strain-softening plasticity, is proposed to prevent loss of ellipticity. Now, numerical solutions result for shear-band formation which are independent of the size and the orientation of the discretisation.

Keywords Non-associated plasticity · Cosserat continuum · Mesh bias · Strain localisation · Shear band · Ellipticity

1 Introduction

Localisation commonly occurs in geomaterials in the form of narrow, highly deformed zones, known as shear bands [39, 42, 52, 53]. Shear bands are considered to emerge from a material instability, i.e. as a bifurcation from a homogeneous deformation into a deformation mode that involves a discontinuity. Hadamard was the first to conduct an analytical study into localisation for elastic solids and has identified the loss of ellipticity as the underlying reason [20]. Extensions to plastic deformations have been made by Hill [22], Mandel [25] and Thomas [46], and it has been established that in addition to strain softening, constitutive features such as the existence of a vertex-like effect in the yield surface, or non-normality of the plastic flow can have a destabilising effect [31, 37, 38, 40, 48, 49].

Supported by ERC Advanced Grant 664734 PoroFrac.

Sepideh Alizadeh Sabet
Department of Civil and Structural Engineering, University of Sheffield, Sheffield, S1 3JD, UK
E-mail: salizadehsabet1@sheffield.ac.uk

René de Borst
Department of Civil and Structural Engineering, University of Sheffield, Sheffield, S1 3JD, UK
E-mail: r.deborst@sheffield.ac.uk

Numerical simulations of localised deformation can run into problems, in particular a pathological mesh dependence, and severe difficulties, or even an impossibility, to obtain converged solutions. In the limiting case of an infinitely dense mesh, failure can occur without energy dissipation, which is physically unrealistic [12]. This pathological mesh dependence happens for any discretisation method as the underlying reason is not the discretisation method, but the ill-posedness of the boundary-value problem due to loss of ellipticity [33, 36]. As said, loss of ellipticity can occur not only due to the strain softening, but it has been shown to also occur for strain-*rate* softening [51] and for non-associated plasticity [9, 31, 41].

Various approaches have been proposed to regularise the problem of strain localisation. Non-local models [5, 6, 35] or gradient continua [13, 29, 34, 47] are regularisation methods which can avoid local loss of ellipticity. Inclusion of viscosity and rate effects have also been proven effective in regularising the boundary-value problem [15, 24, 32]. The Cosserat model [7] is particularly applicable to granular materials as it is capable of taking the microstructure of the material into account via a microrotation, representing the average spin of the particles, as an additional degree of freedom. It has subsequently been used to regularise constitutive models of granular materials [10, 14, 11, 30, 28]. We have recently shown that the use of a Cosserat continuum model also successfully removes mesh size dependency which results from a non-associated plastic flow rule, which is typically used for pressure-sensitive materials [41].

Herein we consider the dependence of numerical results on the mesh orientation. While the effect of mesh orientation has received less attention than the effect which mesh densification can have in localisation problems, its relevance has been documented for strain softening [44], for strain-rate softening in the formation of Portevin-Le Chatelier bands [51] and for softening-rehardening as occurs in Lüders band formation [27]. Now, we focus on the case where the orientation dependence results from the application of a non-associated flow rule. In order to investigate the effect of non-associativity, we exclude all other possible destabilising effects, such as the explicit inclusion of strain softening in the constitutive model, or geometrically destabilising factors. We first recall the underlying mathematical condition which causes loss of ellipticity and it is shown how this condition can be satisfied for a Mohr-Coulomb plasticity model with a non-associated flow embedded in a standard continuum. Next, a numerical example of a biaxial test under compression is considered. Numerical simulations show the dependence of the deformation on the spatial discretisation both in terms of its density and of the direction of the mesh lines. The Cosserat continuum is reviewed next and is used in simulations of the same biaxial test, which now result in objectivity with respect to the mesh size as well as the mesh orientation.

2 Analysis of localisation

2.1 Loss of ellipticity

A mathematical model of a physical problem is reliable only when the initial or boundary value problem is well-posed, since the solution then continuously depends on the data. For quasi-static loading conditions this translates into the requirement that the governing differential equations are elliptic at each point of the continuous medium. We now investigate conditions under which a body which is modelled using non-associated elasto-plasticity, locally loses ellipticity, therefore opening up the possibility of strain localisation to occur. We consider quasi-static loading conditions and postulate the existence of a solution which is discontinuous across a (possibly curved) plane $\mathit{\Gamma}_d$. Assuming a linear comparison solid [21], so that the tangential stiffness tensor $\mathbf{D}$ is identical at both sides of the discontinuity, the jump in the stress rate is related to the jump in the strain rate as:

$$[\![\dot{\boldsymbol{\sigma}}]\!] = \mathbf{D} : [\![\dot{\boldsymbol{\epsilon}}]\!] \tag{1}$$

The jump in the traction rate, $[\![\dot{\mathbf{t}}_d]\!]$, across the plane is expressed as:

$$[\![\dot{\mathbf{t}}_d]\!] = \mathbf{n}_{\mathit{\Gamma}_d} \cdot [\![\dot{\boldsymbol{\sigma}}]\!] \tag{2}$$

where $\mathbf{n}_{\mathit{\Gamma}_d}$ is the normal vector to the discontinuity $\mathit{\Gamma}_d$. Using the expression for $[\![\dot{\boldsymbol{\sigma}}]\!]$ given by Eq. (1), the jump in the traction rate jump reads:

$$[\![\dot{\mathbf{t}}_d]\!] = \mathbf{n}_{\mathit{\Gamma}_d} \cdot \mathbf{D} : [\![\dot{\boldsymbol{\epsilon}}]\!] \tag{3}$$

A velocity field $\dot{\mathbf{u}}$ which contains a discontinuity at $\mathit{\Gamma}_d$ can generally be expressed as:

$$\dot{\mathbf{u}} = \dot{\bar{\mathbf{u}}} + \mathcal{H}_{\mathit{\Gamma}_d} \dot{\tilde{\mathbf{u}}} \tag{4}$$

where $\mathcal{H}_{\mathit{\Gamma}_d}$ is the Heaviside function, and $\dot{\bar{\mathbf{u}}}$ and $\dot{\tilde{\mathbf{u}}}$ are continuous velocity fields on both sides of the discontinuity. Differentiating Eq. (4) results in the strain rate field:

$$\dot{\boldsymbol{\epsilon}} = \nabla^{\text{sym}} \dot{\bar{\mathbf{u}}} + \mathcal{H}_{\mathit{\Gamma}_d} \nabla^{\text{sym}} \dot{\tilde{\mathbf{u}}} + \delta_{\mathit{\Gamma}_d} (\dot{\tilde{\mathbf{u}}} \otimes \mathbf{n}_{\mathit{\Gamma}_d})^{\text{sym}} \tag{5}$$

where $(.)^{\text{sym}}$ refers to the symmetrised part of the operator and $\delta_{\mathit{\Gamma}_d}$ denotes the Dirac function at $\mathit{\Gamma}_d$. The strain rate jump at $\mathit{\Gamma}_d$ can be written as:

$$[\![\dot{\boldsymbol{\epsilon}}]\!] = \zeta \left(\dot{\tilde{\mathbf{u}}} \otimes \mathbf{n}_{\mathit{\Gamma}_d} \right)^{\text{sym}} \tag{6}$$

with ζ a non-zero scalar representing the magnitude of the difference in the strain rate jump. Substitution into Eq. (3) and exploiting the minor symmetry of $\mathbf{D}$ yields:

$$[\![\dot{\mathbf{t}}_d]\!] = \zeta \left(\mathbf{n}_{\mathit{\Gamma}_d} \cdot \mathbf{D} \cdot \mathbf{n}_{\mathit{\Gamma}_d} \right) \cdot \dot{\tilde{\mathbf{u}}} \tag{7}$$

A non-trivial solution ($\zeta \neq 0$) to Eq. (7) exists if and only if the acoustic tensor is is singular:

$$\det \left(\mathbf{n}_{\mathit{\Gamma}_d} \cdot \mathbf{D} \cdot \mathbf{n}_{\mathit{\Gamma}_d} \right) = 0 \tag{8}$$

Eq. (8) is the condition for the existence of discontinuous, localised solutions. It violates the ellipticity condition of the tangential stiffness operator [26]. Eq. (8) also determines the speed at which plane acceleration waves in solids vanish[22].

2.2 Application to non-associated plasticity

The Mohr-Coulomb plasticity model has frequently been used in analyses of strain localisation in geomaterials and the yield function is given by:

$$f = \frac{1}{2}(\sigma_3 - \sigma_1) + \frac{1}{2}(\sigma_3 + \sigma_1)\sin\phi - c\cos\phi \tag{9}$$

while the following expression is normally used as plastic potential:

$$g = \frac{1}{2}(\sigma_3 - \sigma_1) + \frac{1}{2}(\sigma_3 + \sigma_1)\sin\psi \tag{10}$$

Herein, σ_1 and σ_3 are the smallest and the largest principal stresses, respectively, while ϕ, ψ and c are the friction angle, the dilation angle and the cohesion, respectively.

For a Mohr-Coulomb plasticity model with a non-associated flow rule as above, the hardening modulus h has been derived as [4, 40, 50]:

$$\frac{h}{\mu} = \frac{(\sin\phi - \sin\psi)^2 - (2\cos 2\theta - \sin\psi - \sin\phi)^2}{8(1-\nu)} \tag{11}$$

where μ and ν are the shear modulus and Poisson's ratio, respectively, and θ is the angle between the most compressive principal stress and the localised shear band. Eq. (11) is a relation between the hardening modulus and the orientation of a discontinuity in the solution for a given set of material parameters μ, ν, ϕ, ψ. At peak, ellipticity is lost and shear bands can form:

$$\frac{h_{\text{crit}}}{\mu} = \frac{(\sin\phi - \sin\psi)^2}{8(1-\nu)} \tag{12}$$

With Eq. (12), we can examine the conditions which lead to a real solution for h_{crit} with loss of ellipticity, opening up the possibility of mesh sensitive solutions.

For the particular case of a non-associated Mohr-Coulomb elastic-perfectly plastic model, we have $h = 0$ and since $\mu > 0$ and $\nu \leq 1/2$, a range of angles θ can be found for which $h < h_{\text{crit}}$ for non-associated flow, i.e. when $\psi < \phi$. These angles are usually bounded by the classical Coulomb and Roscoe angles [8, 39] which are the roots of the hardening modulus. This is visualised in Figure 1 for a given set of material parameters ($\nu = 0.25$ and $\phi = 25^{\text{o}}$).

2.3 The orientation of shear bands

There are three main approaches to compute the inclination angle of the shear bands. Coulomb [8] considered the orientation angle to be $\theta = 45^{\text{o}} - \phi/2$. Roscoe [39] has derived another solution, namely $\theta = 45^{\text{o}} - \psi/2$, which gives prominence to role of the dilatancy. Another relation, $\theta = 45^{\text{o}} - (\psi + \phi)/4$, was based on experimental data [3]. This relation was also found in experiments on Karlsruhe sand and in an accompanying bifurcation analysis [48]. Considering a wide range of experimental data, Arthur and Dunstan [2] concluded that the shear band varies between the Roscoe and the Coulomb solutions depending on the mean particle size. For coarse-grained sands the Roscoe solution is approached, while for finer grains the Coulomb solution tends to be favoured. These findings were corroborated theoretically [49], and experimentally for specimens with coarse-sized particles [18] and for fine sands [16].

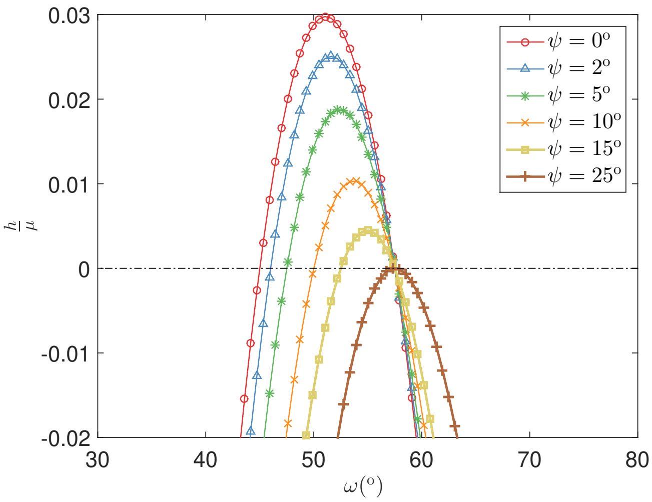

Fig. 1 Hardening modulus *vs* the orientation angle of the shear band, $\omega = \pi/2 - \theta$

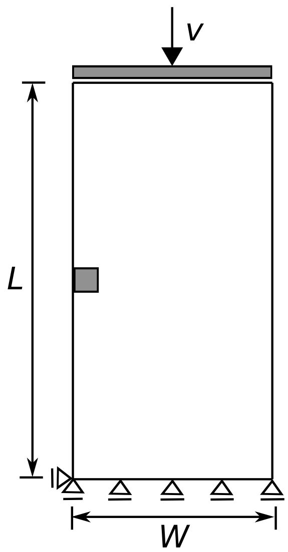

Fig. 2 Geometry with boundary conditions and imperfection

3 Numerical simulations

3.1 Model set-up

A compression biaxial test is considered in order to investigate the influence of the mesh density and the mesh orientation during shear banding. The geometry and the boundary conditions are shown in Figure 2. The dimensions of the specimen are L = 20 cm and W = 10 cm, respectively. A compressive stress field results from a smooth, rigid platen being moved downwards uniformly at the top of the specimen.

3.2 Drucker-Prager plasticity model

The Drucker-Prager yield contour shares the pressure dependence with the Mohr-Coulomb yield contour, but has the advantage in numerical computations that it is only singular at the apex. It is characterised by the yield function [17]:

$$f = \sqrt{3J_2} + \alpha p - k \tag{13}$$

and by the resembling plastic potential:

$$g = \sqrt{3J_2} + \beta p \tag{14}$$

where J_2 is the second invariant of deviatoric stresses and p is the hydrostatic pressure. α and β are the friction coefficient and the dilatancy factor, respectively, while k is related to the cohesive strength. Under plane-strain conditions, the material parameters in the Drucker-Prager model can be related to those of the Mohr-Coulomb model through:

$$\alpha = \frac{6\sin\phi}{3-\sin\phi} \quad , \quad \beta = \frac{6\sin\psi}{3-\sin\psi} \tag{15}$$

The evolution of the plastic strains is governed by a flow rule, as usual:

$$\dot{\boldsymbol{\epsilon}}^p = \dot{\lambda}\frac{\partial g}{\partial \boldsymbol{\sigma}} \tag{16}$$

The plastic multiplier $\dot{\lambda}$ is obtained from the consistency condition ($\dot{f} = 0$) as follows:

$$\dot{\lambda} = \frac{\frac{\partial f}{\partial \boldsymbol{\sigma}} : \mathbf{D}^e : \dot{\boldsymbol{\epsilon}}}{\frac{\partial f}{\partial \boldsymbol{\sigma}} : \mathbf{D}^e : \frac{\partial g}{\partial \boldsymbol{\sigma}}} \tag{17}$$

where $\mathbf{D}^e$ is the elastic stiffness tensor. The rate equations are integrated with a standard implicit return algorithm with a special treatment of the stresses near the apex of the yield surface. A consistent tangent operator has been used to ensure the quadratic convergence rate [12, 45].

A non-associated elastic-ideally plastic Drucker-Prager type material model is considered in the remainder of this paper. The elasticity parameters read: Young's modulus $E = 100$ kPa and Poisson's ratio $\nu = 0.25$. With a friction angle $\phi = 25^{\circ}$ and a dilatancy angle $\psi = 5^{\circ}$, Eq. (15) can be used to compute $\alpha = 0.984$ and $\beta = 0.18$. For the cohesive strength the parameter value $k = 0.06$ kPa has been taken.

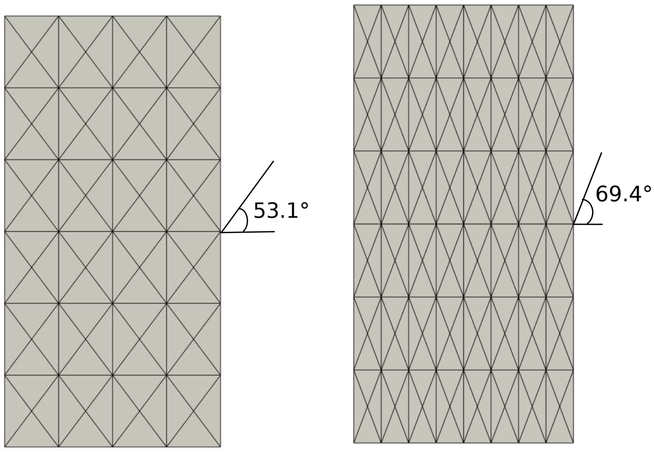

(a) Model A (b) Model B

Fig. 3 Two discretisations with different mesh directions

3.3 Mesh arrangements

In the numerical analyses two different mesh arrangements, model A and model B, have been used, each composed of quadratic triangular elements in a crossed lay-out. Use of these elements avoids the problem of volumetric locking and makes it more convenient to study directional mesh bias. Model A has been analysed for three different mesh sizes, 4×6, 8×12 and 16×24 elements. In model A, the elements have been arranged such that the angle of the element boundaries is at 53.1^o, which is close to the expected direction of shear banding according to the Arthur solution, i.e. 52.5^o for the chosen parameter set, see Section 2. In model B, the diagonals of the mesh are very different at a value of 69.4^o, see Figure 3. Three different discretisation levels have also been considered now, 8×6, 16×12 and 32×24.

To induce a non-homogeneous stress field and hence to trigger localisation, an imperfect element with a 16.7% reduction in the cohesive strength has been inserted at the left boundary, just above the centre line in both models.

4 Shear banding in a standard elasto-plastic continuum

4.1 Sensitivity to mesh size

Localisation zones develop starting from the imperfection and continue to grow until a peak in the load-displacement curve, Figure 4, has been reached. At this point loss of ellipticity occurs and the boundary-value problem becomes ill-posed. A post-peak structural softening is observed for all discretisations of model A. The slope of the softening becomes steeper upon mesh refinement. It is emphasised that the structural softening is here purely a consequence of the use of a non-associated

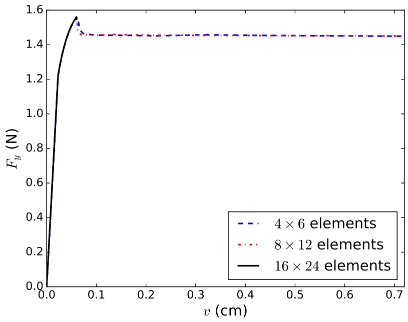

(a) Full curve

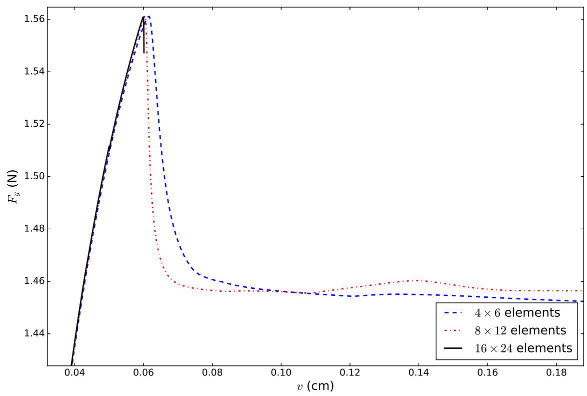

(b) Zoom post-peak

Fig. 4 Load-displacement curve for model A using a standard Drucker-Prager model

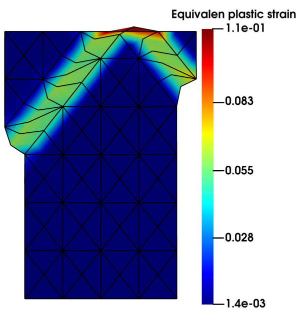

(a) 4×6 elements

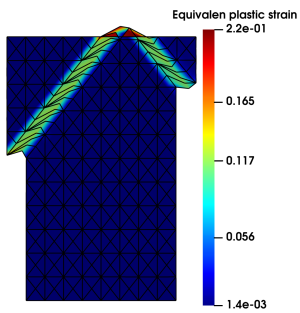

(b) 8×12 elements

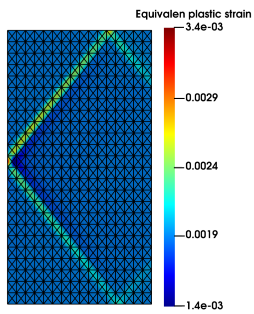

(c) 16×24 elements

Fig. 5 Equivalent plastic strain for model A, a) and b) at $v = 0.2$ cm, c) shortly before the iterative solution fails, at $v = 0.06$ cm

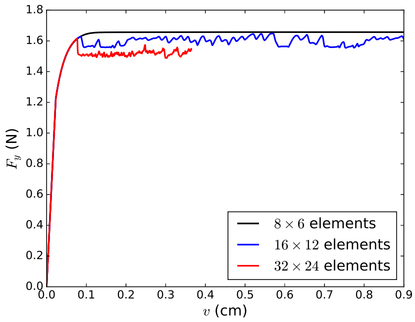

Fig. 6 Load-displacement curve for model B using a standard Drucker-Prager model

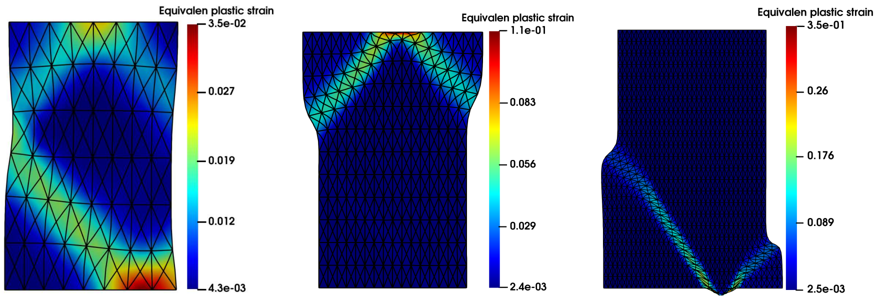

(a) 8×6 elements (b) 16×12 elements (c) 32×24 elements

Fig. 7 Equivalent plastic strain for model B, at $v = 0.2$ cm, using a standard Drucker-Prager model

flow rule, and has been observed before in computations [9] and has been analysed in depth [23, 41].

Since the boundary-value problem becomes ill-posed at this point obtaining a converged solution becomes difficult. Indeed, for the fine mesh of model A divergence occurs shortly after the peak load even for extremely small load steps. A possible reason is that snap-back behaviour may occur which cannot be resolved under displacement control.

From Figure 5 it can be seen that in model A a highly localised shear band is formed and that the size of the shear band is dominated by the mesh size. The shear band is confined to a single band of elements. If the element size approaches zero, the shear band width would also becomes zero and the load-displacement curve would double back on the loading branch, resulting in a physically meaningless solution with zero energy dissipation [12].

The results for model B also show post-peak structural softening, but only for the finer discretisations (16×12 and 32×24), see Figure 6. A poor convergence behaviour with severe oscillations is observed upon mesh refinement. Indeed, for the finest mesh the solution procedure breaks down after reaching a plateau. The residual load level, i.e. the load level which is reached after structural softening, is slightly higher in model B than in model A. A shear band also forms in model B, but is considerably more diffuse than in model A, see Figure 7.

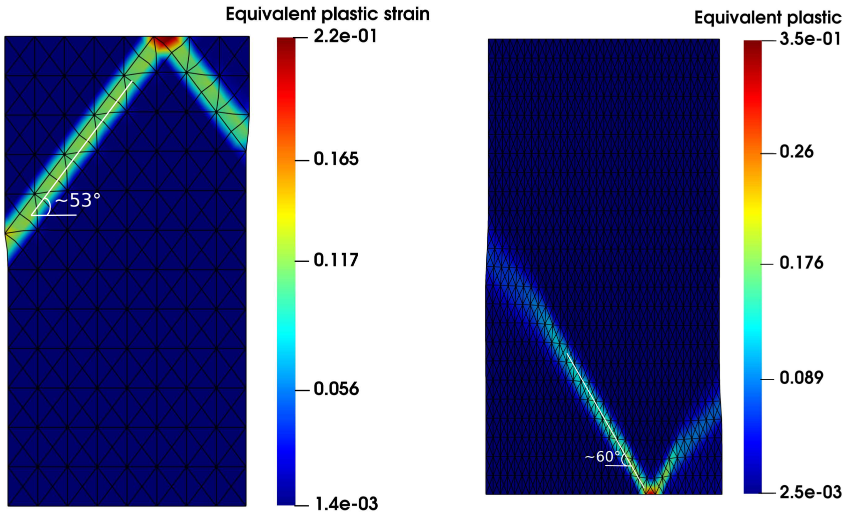

(a) Model A (b) Model B

Fig. 8 Shear band orientation in model A *vs* model B

4.2 Sensitivity to mesh alignment

Figure 8 shows the bias of the initial element arrangement on the shear band. In model A shear band formation occurs along the edges of the elements, and therefore, the orientation is dominated by the mesh diagonals, i.e. at $\omega = 53^{\circ}$, which is close to the Arthur solution, $\omega = 45^{\circ} + (\phi + \psi)/4 = 52.5^{\circ}$ [3]. It is emphasised that this correct inclination has been helped by the initial mesh layout, with diagonals at $\omega = 53.1^{\circ}$, cf. Section 3. For model B the angle at which the shear band forms is also influenced by the mesh orientation, and shear bands form at $\omega = 60^{\circ}$ degrees. This difference shows how the mesh orientation can bias the solution for ill-posed boundary value problems.

5 Cosserat elasto-plasticity

In the preceding it has been demonstrated how a standard continuum suffers from a local loss of ellipticity at the onset of localisation, which leads to mesh dependence both in terms of the size and the orientation. A Cosserat continuum model has been used before to eliminate mesh dependence due to strain softening in the constitutive model, [10, 11, 14] and has also been used to predict the thickness of shear bands as a function of the grain size [30]. Herein, we examine whether a Cosserat continuum model is also effective in preventing loss of ellipticity and ensuing mesh alignment dependency for non-associated plasticity.

5.1 Model summary

In the absense of inertia terms and body forces the balance of linear momentum and of moment of momentum of a Cosserat continuum can be formulated as [1, 43]:

$$\operatorname{div} \boldsymbol{\sigma}^{\mathrm{T}} = \mathbf{0} \tag{18}$$

and

$$\operatorname{div} \mathbf{m}^{\mathrm{T}} + \boldsymbol{e} : \boldsymbol{\sigma} = \mathbf{0} \tag{19}$$

respectively, where $\boldsymbol{\sigma}$ is the Cauchy stress tensor, $\mathbf{m}$ is the couple-stress tensor, and $\boldsymbol{e}$ is the permutation tensor.

From the the usual displacement vector $\mathbf{u}$ and a micro-rotation vector $\boldsymbol{\omega}$ the strain tensor $\boldsymbol{\epsilon}$ and a micro-curvature tensor $\boldsymbol{\kappa}$ can be derived, which are conjugate to the Cauchy stress tensor and the couple-stress tensor, respectively,

$$\boldsymbol{\epsilon} = \nabla \mathbf{u} - \boldsymbol{e} \cdot \boldsymbol{\omega} \tag{20}$$

and

$$\boldsymbol{\kappa} = \nabla \boldsymbol{\omega} \tag{21}$$

Under the usual small-strain assumption, the strain tensor is decomposed additively into an elastic and a plastic part,

$$\boldsymbol{\epsilon} = \boldsymbol{\epsilon}^{e} + \boldsymbol{\epsilon}^{p} \tag{22}$$

augmented by a similar relation for the micro-curvatures:

$$\boldsymbol{\kappa} = \boldsymbol{\kappa}^{e} + \boldsymbol{\kappa}^{p} \tag{23}$$

A linear relationship exists between the elastic parts of the strain and the micro-curvature tensors on one hand, and the stress and couple-stress tensors on the other hand:

$$\boldsymbol{\sigma} = \frac{2\nu\, \mu \operatorname{tr}(\boldsymbol{\epsilon}^{e})}{1 - 2\nu}\, \mathbf{I} + (\mu + \mu_c)\, \boldsymbol{\epsilon}^{e} + \mu\, (\boldsymbol{\epsilon}^{e})^{\mathrm{T}} \tag{24}$$

and

$$\mathbf{m} = \mu \left(\ell_1^2\, \boldsymbol{\kappa}^{e} + \ell_2^2\, (\boldsymbol{\kappa}^{e})^{\mathrm{T}} + \ell_3^2 \operatorname{tr}(\boldsymbol{\kappa}^{e})\, \mathbf{I} \right) \tag{25}$$

where $\mathbf{I}$ is the second-order identity tensor, and μ_c, ℓ_1, ℓ_2 and ℓ_3 are additional material parameters. The last two terms in Eq. (25) cancel in case of planar deformations, and a reduced expression is obtained:

$$\mathbf{m} = \mu \ell^2\, \boldsymbol{\kappa}^{e} \tag{26}$$

where $\ell_1 = \ell$ is an internal length parameter which influences the width of the localisation zone.

A non-associated Drucker-Prager type perfect-plasticity model is considered as in Eq. (13), with a generalised form of the second invariant of deviatoric stresses as [30]:

$$J_2 = a_1\, \mathbf{s}^{\mathrm{T}} : \mathbf{s} + a_2\, \mathbf{s} : \mathbf{s} + a_3\, \mathbf{m}^{\mathrm{T}} : \mathbf{m}/\ell^2 \tag{27}$$

where s_{ij} are the components of the deviatoric stress tensor, and the constraint $a_1 + a_2 = \frac{1}{2}$ must hold for the classical expression for J_2 to be retrieved in the absence of couple-stress tensors. It has been shown that the values $a_1 = \frac{1}{4}$, $a_2 = \frac{1}{4}$

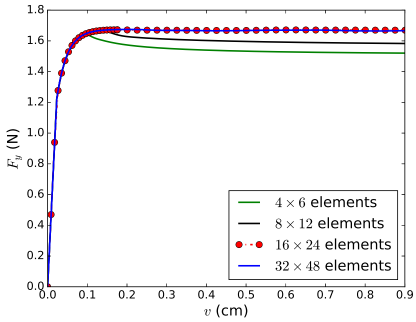

Fig. 9 Load-displacement curve for model A using Cosserat plasticity

and $a_3 = \frac{1}{2}$ result in a particularly simple numerical algorithm [10, 11]. The plastic potential is similar to that introduced in Eq. (14), now employing the generalised J_2, Eq. (27). The stress integration procedure is carried out in a similar fashion as in classical plasticity.

Here, another advantage of using the Drucker-Prager yield contour becomes apparent. The extension from a standard continuum to a Cosserat continuum model is simple and straightforward, and merely requires the re-definition of some stress and plastic strain invariants.

5.2 Computations with Cosserat elasto-plasticity

The biaxial test considered in Section 3 has bee re-analysed using Cosserat elasto-plasticity. The set-up and material parameters are as before. Two additional material parameters, $\mu_c = 20$ kPa and a characteristic length $\ell = 1$ mm have been adopted for the Cosserat model. The parameter values have been chosen such that they properly bring out the regularising effect without requiring an overly dense discretisation. A procedure to determine the additional material parameters in a Cosserat continuum has been described in [19].

Model A has been analysed with four different levels of mesh refinement, 4×6, 8×12, 16×24, 32×48 elements and model B has been analysed for the same discretisations as before.

5.3 Objectivity with respect to the mesh density

The load-displacement curves for models A and B are shown in Figures 9 and 10, respectively. They show that in both models the results converge to a unique solution upon refinement of the discretisation, which is in contrast to the results for standard non-associated Drucker-Prager plasticity. For a sufficient refinement level, the width of the shear bands is not affected by the mesh size, neither in model A, nor in model B. Figure 11 also shows that the solutions of models A and B then agree well. For the assumed characteristic length scale, a mild structural softening occurs, but this is no longer mesh-dependent after a converged solution has been obtained. The equivalent plastic strain contours, see Figures 12 and 13,

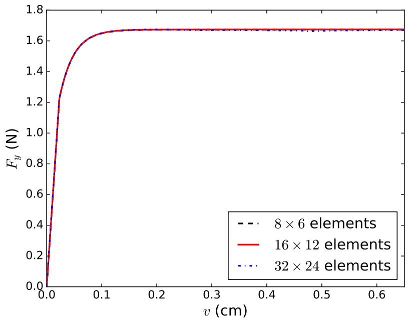

Fig. 10 Load-displacement curve for model B using Cosserat plasticity

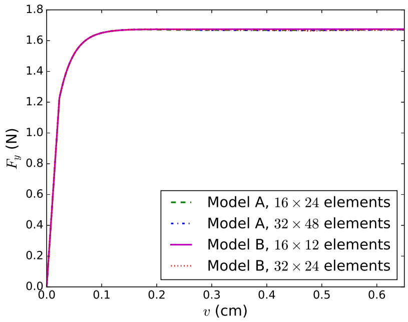

(a) Full curve

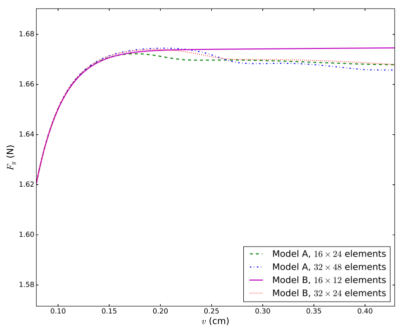

(b) Zoom post-peak

Fig. 11 Load-displacement curve using Cosserat plasticity

also show that strains are not localised over a single layer of elements, but over a shear band with a finite width of approximately 16 mm, which makes that the ratio of the shear band width over the internal length scale is in the range of established theoretical values [30] and experimental observations [48].

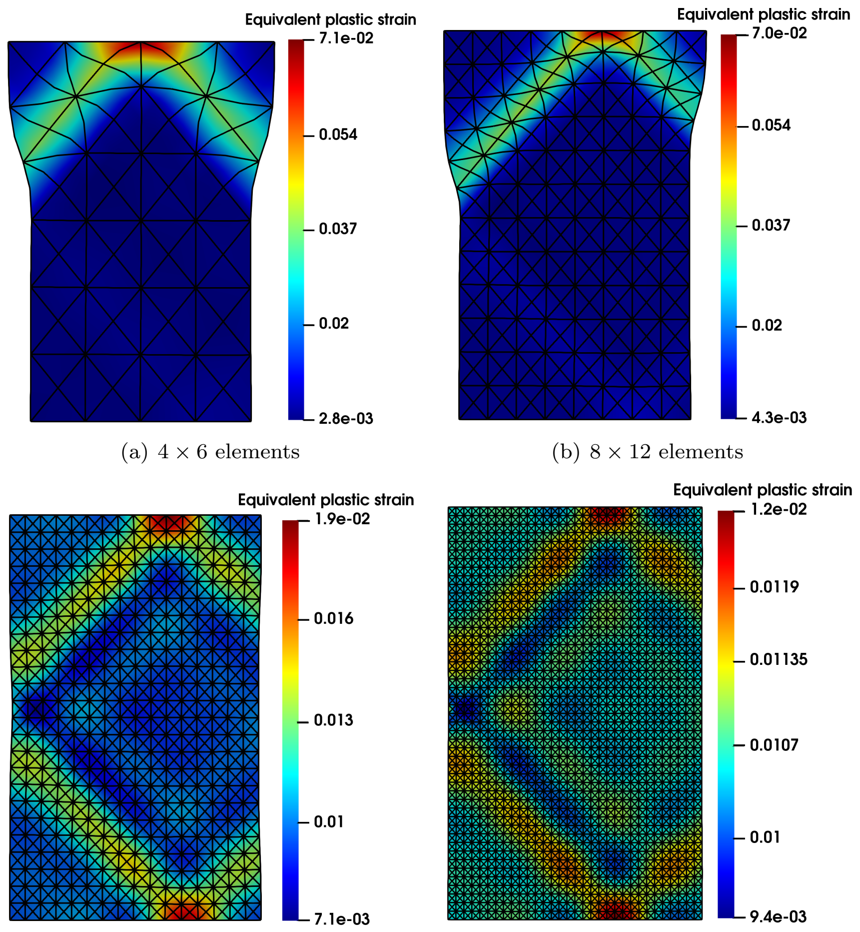

(a) 4 × 6 elements (b) 8 × 12 elements

(c) 16 × 24 elements (d) 32 × 48 elements

Fig. 12 Equivalent plastic strain for model A, at $v = 0.2$ cm, using Cosserat Drucker-Prager plasticity

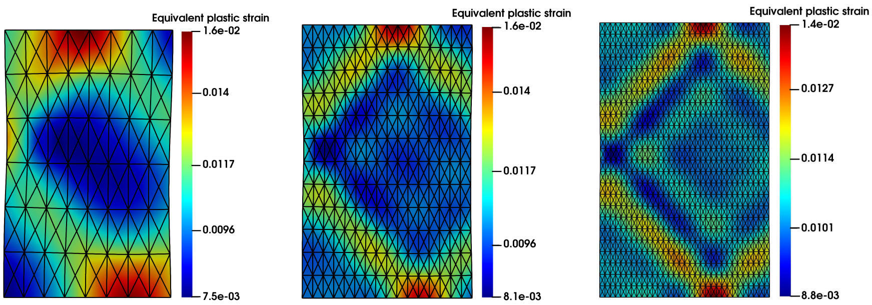

(a) 4 × 6 elements (b) 8 × 12 elements (c) 16 × 24 elements

Fig. 13 Equivalent plastic strain for model B, at $v = 0.2$ cm, using Cosserat Drucker-Prager plasticity

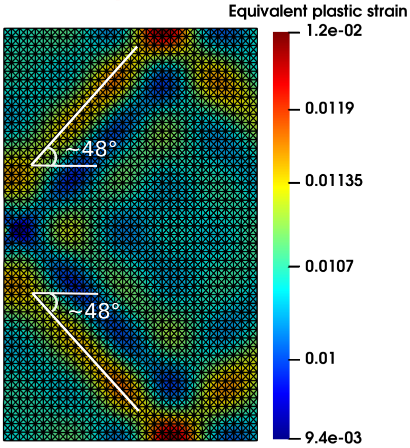

(a) Model A

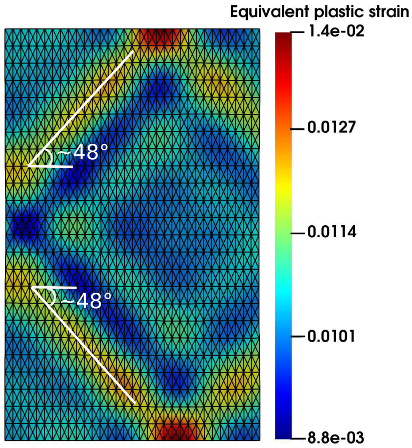

(b) Model B

Fig. 14 Shear band angles for both models (A and B) using Cosserat plasticity

5.4 Objectivity with respect to the orientation of the mesh lines

Comparing Figures 12 and 13 reveals a very similar shear band pattern and orientation angle for both models after sufficient refinement. Upon mesh refinement each model converges to a unique solution, and there is a very good agreement in terms of the inclination angle of the shear band. The observed shear band patterning is characteristic for the use of a Cosserat continuum model.

5.5 Shear-band orientation

The shear bands form at approximately $\omega = 48^{\text{o}}$ both in model A and in model B when using Cosserat Drucker-Prager plasticity, as shown in Figure 14. This is different from the shear band inclination angles from classical bifurcation theory, which rather suggest $\omega = 52.5^{\text{o}}$. In fact, they closer match the Roscoe solution ($\omega = 45^{\text{o}} + \psi/2 = 47.5^{\text{o}}$). This suggests that the introduction of an internal length scale to represent the grain size can result in a reproduction of the experimental observation that the inclination angle depends on the grain size [16, 18].

6 Concluding remarks

Non-associated plasticity can lead to loss of ellipticity at a generic stage in the loading process. This leads to mesh-dependent solutions. Herein, we have shown that this mesh dependence not only relates to the mesh density, but also to the orientation of the mesh lines, as shear bands tend to follow the mesh lines.

Regularisation, in this case by means of a Cosserat continuum which is very applicable to granular materials, prevents loss of ellipticity to occur. As a result, computations become independent of the discretisation, and shear bands are no longer biased by the discretisation, neither in terms of density, nor in terms of orientation of the mesh lines. As an added benefit, computability and convergence of the iterative procedure to solve the set of non-linear equations are vastly improved.

Acknowledgements Financial support of the European Research Council under Advanced Grant 664734 'PoroFrac' is gratefully acknowledged.

References

1. Altenbach, H., Eremeyev, V.A.: Cosserat media. In: Generalized Continua – From the Theory to Engineering Applications, pp. 65–130. Springer-Verlag, Wien - Heidelberg - New York - Dordrecht - London (2013)
2. Arthur, J.R.F., Dunstan, T.: Rupture layers in granular media. In: P.A. Vermeer, H.J. Luger (eds.) Proceedings IUTAM Symposium on Deformation and Failure in Granular Media, pp. 453–460. A. A. Balkema, Rotterdam (1982)
3. Arthur, J.R.F., Dunstan, T., Al-Ani, Q.A.J.L., Assadi, A.: Plastic deformation and failure in granular media. Géotechnique **27**, 53–74 (1977)
4. Bardet, J.P.: A comprehensive review of strain localization in elastoplastic soils. Computers and Geotechnics **10**, 163–188 (1990)
5. Bažant, Z.P., Belytschko, T.B., Chang, T.P.: Continuum theory for strain-softening. ASCE Journal of Engineering Mechanics **110**, 1666–1692 (1984)
6. Bažant, Z.P., Pijaudier-Cabot, G.: Nonlocal continuum damage, localization instability and convergence. ASME Journal of Applied Mechanics **55**, 287–293 (1988)
7. Cosserat, E., Cosserat, F.: Théorie des Corps Déformables. A. Hermann et fils, Paris (1909)
8. Coulomb, C.A.: Essai sur une application des règles des maximis et minimis à quelques problemès de statique. Memoires Académie Royale des Sciences **7**, 343–382 (1776)
9. de Borst, R.: Bifurcations in finite element models with a non-associated flow law. International Journal for Numerical and Analytical Methods in Geomechanics **12**, 99–116 (1988)
10. de Borst, R.: Simulation of strain localization: A reappraisal of the Cosserat continuum. Engineering Computations **8**, 317–332 (1991)
11. de Borst, R.: A generalisation of J2-flow theory for polar continua. Computer Methods in Applied Mechanics and Engineering **103**, 347–362 (1993)
12. de Borst, R., Crisfield, M.A., Remmers, J.J.C., Verhoosel, C.V.: Nonlinear Finite Element Analysis of Solids and Structures. John Wiley & Sons, Chichester (2012)
13. de Borst, R., Mühlhaus, H.B.: Gradient-dependent plasticity: formulation and algorithmic aspects. International Journal for Numerical Methods in Engineering **35**, 521–539 (1992)
14. de Borst, R., Sluys, L.J.: Localisation in a Cosserat continuum under static and dynamic loading conditions. Computer Methods in Applied Mechanics and Engineering **90**, 805–827 (1991)

15. de Borst, R., Sluys, L.J., Mühlhaus, H.B., Pamin, J.: Fundamental issues in finite element analysis of localisation of deformation. Engineering Computations **10**, 99–122 (1993)
16. Desrues, J.: La localisation de la déformation dans les matériaux granulaires. Ph.D. thesis, Institut National Polytechnique de Grenoble, Grenoble (1984)
17. Drucker, D.C., Prager, W.: Soil mechanics and plastic analysis or limit design. Quarterly of Applied Mathematics **10**, 157–165 (1952)
18. Duthilleul, B.: Rupture progressive: Simulation physique et numérique. Ph.D. thesis, Institut National Polytechnique de Grenoble, Grenoble (1983)
19. Ehlers, W., Scholz, B.: An inverse algorithm for the identification and the sensitivity analysis of the parameters governing micropolar elasto-plastic granular material. Archive of Applied Mechanics **77**, 911–931 (2007)
20. Hadamard, J.: Leçons sur la Propagation des Ondes et les Équations de l'Hydrodynamique. A. Hermann, Paris (1903)
21. Hill, R.: A general theory of uniqueness and stability in elastic-plastic solids. Journal of the Mechanics and Physics of Solids **6**, 236–249 (1958)
22. Hill, R.: Acceleration waves in solid. Journal of the Mechanics and Physics of Solids **10**, 1–16 (1962)
23. Le Pourhiet, L.: Strain localization due to structural softening during pressure sensitive rate independent yielding. Bulletin de la Société géologique de France **184**, 357–371 (2013)
24. Loret, B., Prévost, J.H.: Dynamic strain localization in elasto-(visco-) plastic solids, Part 1. General formulation and one-dimensional examples. Computer Methods in Applied Mechanics and Engineering **83**, 247–273 (1990)
25. Mandel, J.: Conditions de stabilité et postulat de Drucker. In: C.J. Kravtchenko, P.M. Sirieys (eds.) Proceedings IUTAM Symposium on Rheology and Soil Mechanics, pp. 58–68. Springer-Verlag, Berlin (1966)
26. Marsden, J.E., Hughes, T.J.R.: Mathematical Foundations of Elasticity. Prentice Hall, Englewood Cliffs, New Jersey (1983)
27. Mazière, M., Forest, S.: Strain gradient plasticity modeling and finite element simulation of Lüders band formation and propagation. Continuum Mechanics and Thermodynamics **27**, 83–104 (2015)
28. Mühlhaus, H.B.: Application of Cosserat theory in numerical solutions of limit load problems. Ingenieur-Archiv **59**, 124–137 (1989)
29. Mühlhaus, H.B., Aifantis, E.C.: A variational principle for gradient plasticity. International Journal of Solids and Structures **28**, 845–857 (1991)
30. Mühlhaus, H.B., Vardoulakis, I.: The thickness of shear bands in granular materials. Géotechnique **37**, 271–283 (1987)
31. Needleman, A.: Non-normality and bifurcation in plane strain tension and compression. Journal of the Mechanics and Physics of Solids **27**, 231–254 (1979)
32. Needleman, A.: Material rate dependence and mesh sensitivity in localization problems. Computer Methods in Applied Mechanics and Engineering **67**, 69–85 (1988)
33. Pamin, J., Askes, H., de Borst, R.: Two gradient plasticity theories discretized with the element-free Galerkin method. Computer Methods in Applied Mechanics and Engineering **192**, 2377–2407 (2003)
34. Peerlings, R.H.J., de Borst, R., Brekelmans, W.A.M., De Vree, J.H.P.: Gradient enhanced damage for quasi-brittle materials. International Journal for

Numerical Methods in Engineering **39**, 3391–3403 (1996)
35. Pijaudier-Cabot, G., Bažant, Z.P.: Nonlocal damage theory. ASCE Journal of Engineering Mechanics **113**, 1512–1533 (1987)
36. Read, H.E., Hegemier, G.A.: Strain softening of rock, soil and concrete – a review article. Mechanics of Materials **3**, 271–294 (1984)
37. Rice, J.R.: The localization of plastic deformation. In: W.T. Koiter (ed.) Proceedings of the 14th International Congress on Theoretical and Applied Mechanics, pp. 207–220. North-Holland, Amsterdam (1976)
38. Rice, J.R., Rudnicki, J.W.: A note on some features of the theory of localization of deformation. International Journal of Solids and Structures **16**, 597–605 (1980)
39. Roscoe, K.H.: The influence of strains in soil mechanics. Géotechnique **20**, 129–170 (1970)
40. Rudnicki, J.W., Rice, J.R.: Conditions for the localization of deformation in pressure sensitive dilatant materials. Journal of the Mechanics and Physics of Solids **23**, 371–394 (1975)
41. Sabet, S.A., de Borst, R.: Structural softening, mesh dependence, and regularisation in non-associated plastic flow. International Journal for Numerical and Analytical Methods in Geomechanics **43**, 2170–2183 (2019)
42. Scarpelli, G., Wood, D.M.: Experimental observations of shear patterns in direct shear tests. In: P.A. Vermeer, H.J. Luger (eds.) Proceedings IUTAM Symposium on Deformation and Failure in Granular Media, pp. 473–483. A. A. Balkema, Rotterdam (1982)
43. Schaefer, H.: Das Cosserat-Kontinuum. Zeitschrift für Angewandte Mathematik und Mechanik **47**, 485–498 (1967)
44. Sluys, L.J.: Wave propagation, localisation and dispersion in softening solids. Ph.D. thesis, TU Delft, Delft (1992)
45. de Souza Neto, E.A., Peric, D., Owen, D.R.J.: Computational Methods for Plasticity: Theory and Applications. John Wiley & Sons, Chichester (2011)
46. Thomas, T.Y.: Plastic Flow and Fracture in Solids. Academic Press (1961)
47. Triantafyllidis, N., Aifantis, E.C.: A gradient approach to localization of deformation. I. hyperelastic materials. Journal of Elasticity **16**, 225–237 (1986)
48. Vardoulakis, I.: Shear band inclination and shear modulus of sand in biaxial tests. International Journal for Numerical and Analytical Methods in Geomechanics **4**, 103–119 (1980)
49. Vermeer, P.A.: The orientation of shear bands in biaxial tests. Géotechnique **40**, 223–234 (1990)
50. Vermeer, P.A., de Borst, R.: Non-associated plasticity for soils, concrete and rock. Heron **29**, 3–64 (1984)
51. Wang, W.M., Sluys, L.J., de Borst, R.: Viscoplasticity for instabilities due to strain softening and strain-rate softening. International Journal for Numerical Methods in Engineering **40**, 3839–3864 (1997)
52. Wawersik, W.R., Brace, W.F.: Post-failure behavior of a granite and diabase. Rock Mechanics **3**, 61–85 (1971)
53. Wawersik, W.R., Fairhurst, C.H.: A study of brittle rock fracture in laboratory compression experiments. International Journal of Rock Mechanics and Mining Sciences & Geomechanics Abstracts **7**, 561–575 (1970)